Three-dimensional image of tubulin in zinc-induced sheets, reconstructed from electron micrographs

L. A. Amos and T. S. Baker*

*Medical Research Council Laboratory of Molecular Biology, Hills Road, Cambridge CB2 2QH, UK and *Rosenstiel Basic Medical Science Research Center, Brandeis University, Waltham, Mass. 02154, USA*

(Received 4 May 1979)

A three-dimensional image of zinc-induced brain tubulin sheets has been reconstructed by computer from digitized electron microscope images of negatively stained specimens. Different views of the sheets were obtained by tilting the specimens in the microscope and also by sectioning normal to the plane of the sheets. The overall resolution of the data is about 2 nm. The features of the resulting three-dimensional model suggest an explanation for the somewhat variable appearance of tubulin subunits in electron microscope images of negatively stained intact and opened-out microtubules.

Introduction

Analysis of the three-dimensional structure of intact eukaryotic microtubules has so far been limited to a resolution of about 4 nm. The problems, both in the case of imaging individual specimens by electron microscopy[1-3] and in the case of X-ray diffraction of oriented gels of microtubules[4-6] is that the helical symmetry of microtubules is fairly low, with only 13 independent views of the subunits in one image of a whole microtubule. This leads to overlap of different contributions at relatively low resolutions in all microtubule diffraction patterns, whether they are obtained directly by X-ray diffraction, or by optical diffraction of electron microscope images. In the case of X-ray diffraction, there is of course the additional problem that, without additional data (for example, from heavy atom derivatives of the structure), even the relative phases of the non-overlapping contributions are unknown.

In principle, greater resolution information could be obtained by electron microscopy from a small series of images showing individual microtubules tilted through small angles to provide further independent views of the subunits. In practice, it has been found difficult to prepare specimens so that the helical symmetry is well preserved in three dimensions. This appears to be because of a tendency for the microtubules to shrink down towards the support grid as a result of dehydration. But without the help of helical symmetry, a large number of different views is required to reconstruct a three-dimensional density distribution. Extended crystalline sheets of tubulin provide specimens more suitable for the latter type of image analysis, since the information in each view can be averaged over a large number of repeating units in two dimensions to improve the ratio of signal to noise. This allows data from different views to be combined more reliably. Suitably large arrays of tubulin protofilaments assemble when zinc ions are added to buffers normally used for microtubule reassembly[7,8].

The projected structure of the zinc-induced sheets in negative stain has been studied in some detail in two-dimensional projection[9-11]. It appears that these sheets are made up of parallel arrays of the same longitudinal protofilaments that constitute normal microtubules, but that the protofilaments are arranged with alternating polarity, rather than all having the same longitudinal polarity as in a microtubule[1]. In fact, a zinc-induced sheet has $P2_1$ symmetry, with screw dyad axes in the central plane of the sheet and normal to the protofilaments[10]. The projected images clearly show each protofilament to be made up of pairs of 4 nm × 5 nm globular subunits, believed to represent individual α and β tubulin monomers; thus confirming the result suggested by the low resolution structural analysis of flagellar microtubules[1]. The images of the subunits in zinc-induced sheets agree well with those obtained from normal sheets, or opened-out microtubules[9], suggesting that the structure of the protofilaments is fairly constant and that the angular view they present is similar in both types of sheet structure. The latter conclusion is supported by the observation that the interprotofilament spacing is essentially identical in both types of sheet.

This paper describes the reconstruction of a three-dimensional image of negatively stained zinc-induced sheets, from a series of tilted views, following the general principles proposed by DeRosier and Klug[12] and first put into practice for studying the three-dimensional structure of two-dimensional crystalline arrays by Henderson and Unwin[13]. As the tubulin sheets are smaller in extent and appear to be more radiation sensitive than the arrays of *Halobacterium* purple membrane, whose unstained structure Henderson and Unwin were able to analyse to 0.7 nm resolution[13], this present study has been restricted to a lower resolution (to about 2 nm) analysis of negatively stained specimens, that is, sheets embedded in a thin layer of electron-dense stain. Staining has the advantage of greatly increasing the contrast between the protein and its surroundings, but does mean that we are studying the density distribution of stain rather than of the protein itself. The resolution limit we encounter is probably set by

0141 8130/79/040146 11$2.00

the properties of the negative stain and its interaction with the protein. The data are dependent on the way in which the stain covers the surfaces of the protein molecules and penetrates spaces between them. Also, the apparent shapes of the protein molecules may be distorted by interaction with the stain both in the hydrated state and during the dehydration which occurs during specimen preparation. Nevertheless, the resulting three-dimensional model, which has been briefly described[14], has been shown to give quite reasonable agreement with data obtained by X-ray diffraction of microtubules in hydrated gels[5,6]. The present paper gives details of the three-dimensional data collection and analysis.

Experimental

Electron microscopy

Negatively stained specimens were prepared from bovine brain as previously described[10]. Also as before, the specimens were imaged by minimum beam electron microscopy, following the technique of Unwin and Henderson[15]. Low dose images (approximately 500 electrons/nm^2) of tilted specimens were obtained by placing carbon-covered electron microscope grids, supporting negatively stained specimens in random orientations, in specially tilted specimen holders[15], with fixed tilt angles of 21 , 35 and 51 . Images were photographed at a nominal magnification of 25 000 ×.

Some of the grids of negatively stained specimens, after being scanned in the electron microscope as described above, were embedded in Araldite and sectioned normal to their surface. It was found necessary to mount the embedded grids horizontally rather than vertically, for sectioning from above; otherwise the floated sections invariably split along the sliver of grid. The sections were picked up on uncoated grids and viewed without further staining.

Analysis of individual images

Images were screened by optical diffraction to select those with a high degree of order and a suitable degree of underfocus (see below). Even in images of highly tilted specimens, it was possible to identify the orientation of the protofilaments and thereby index the intensity maxima in the diffraction patterns. The problem of whether an image should be turned upside-down or not, to bring it into precisely the same relative orientation as the others, could not be solved at this stage but had to await phase information.

The selected images were digitised by densitometering part of each electron micrograph on a square raster, at intervals corresponding to about 0.4 nm, and 512 × 512 point Fourier transforms were calculated from 512 × 512 point image arrays as described previously[10]. The resulting planes through reciprocal space were thus sampled on a square grid with spacings of about 0.005 nm^{-1}. Points of the reciprocal lattice were separated by 20–30 of these grid spacings. A value for the relative phase at each lattice point (h, k) was obtained by interpolation from the complex values at the nearest four grid points. A value for the intensity at the lattice point was calculated by averaging the intensities (squares of calculated amplitudes) at all the points within a radius of two grid spaces from the calculated position of the lattice point. The background intensity in the region of the lattice point was estimated in a similar way by averaging over points in the annulus between radii of 2 grid spaces and 4 grid spaces. Thus, an amplitude value for the lattice point, corrected for background noise was obtained from the square root of the difference between these two averages. This background correction was felt to be necessary in the present work because the individual images could not be so highly selected for quality as in the two-dimensional study[10], nor could each point in 3-D reciprocal space be averaged over a sufficiently large number of samples to render the noise contribution negligible. No attempt was made to correct the amplitudes for the non-uniformity of the contrast transfer function, which tends to reduce the effect of high resolution features[16]. Phase corrections were not required, since only diffraction patterns in which all the required reflections fell within the first maximum of the contrast transfer function were used in the analysis.

Combination of data from different images

As discussed by others[13], the three-dimensional Fourier transform of a crystal only one unit cell thick in one direction consists of continuous lines of intensity maxima parallel to that axis. As diagrammed in *Figure* 1 for the case of Zn-tubulin sheets, the diffraction pattern from each electron microscope image (being a simple projection of the 3-D structure, in the case of thin biological specimens — see Erickson and Klug[16]) constitutes a central plane through the 3-D Fourier transform, cutting each of the lattice lines at one point. (Although, in the present case, because of the $P2_1$ symmetry of the sheets, values at a second point along each line can be derived from the intersection of the plane with the symmetry-related line — see caption to *Figure* 1).

The distance along a particular lattice line, $Z(h, k)$, of the point of intersection depends on the angle (θ), between the tilt axis and the protofilament axes (as viewed before tilting), and the tilt angle (ψ):

$$Z(h, k) = (h\mathrm{a}^* \cos\theta + k\mathrm{b}^* \sin\theta) \tan\psi \qquad (3)$$

where a* and b* are the reciprocal cell dimensions in the directions of the h and k axes.

We determined the value of θ for each micrograph, from the measured angle, θ', between the tilt axis and the protofilament direction as it appeared in the image (i.e. after tilting), from:

$$\tan\theta = \tan\theta'/\cos\psi \qquad (4)$$

The value of the tilt angle, ψ, for each set of tilted images was checked by measuring the apparent reciprocal cell parameters, a*′, b*′ and $\gamma^{*\prime}$, in their optical transforms, since:

$$\begin{aligned} \tan(\gamma^{*\prime} - \theta') &= \tan(\gamma^* - \theta)\cos\psi \\ \mathrm{a}^{*\prime} &= \mathrm{a}^*(1 + \cos\theta \tan\psi)^{1/2} \\ \mathrm{b}^{*\prime} &= \mathrm{b}^*(1 + \sin\theta \tan\psi)^{1/2} \end{aligned} \qquad (5)$$

where $\mathrm{a}^* = 1/9.8$ nm^{-1}, $\mathrm{b}^* = 1/8.2$ nm^{-1}, $\gamma^* = 90$ (Reference 10).

The sampling required to adequately define the variations in amplitude and phase along the lines in reciprocal space is related to the thickness of the structure[13,17]. As our sheets are less than 10 nm thick (since X-ray diffraction data suggest that the difference between the inner and outer radii of a microtubule is 7–8 nm[4–6]), we

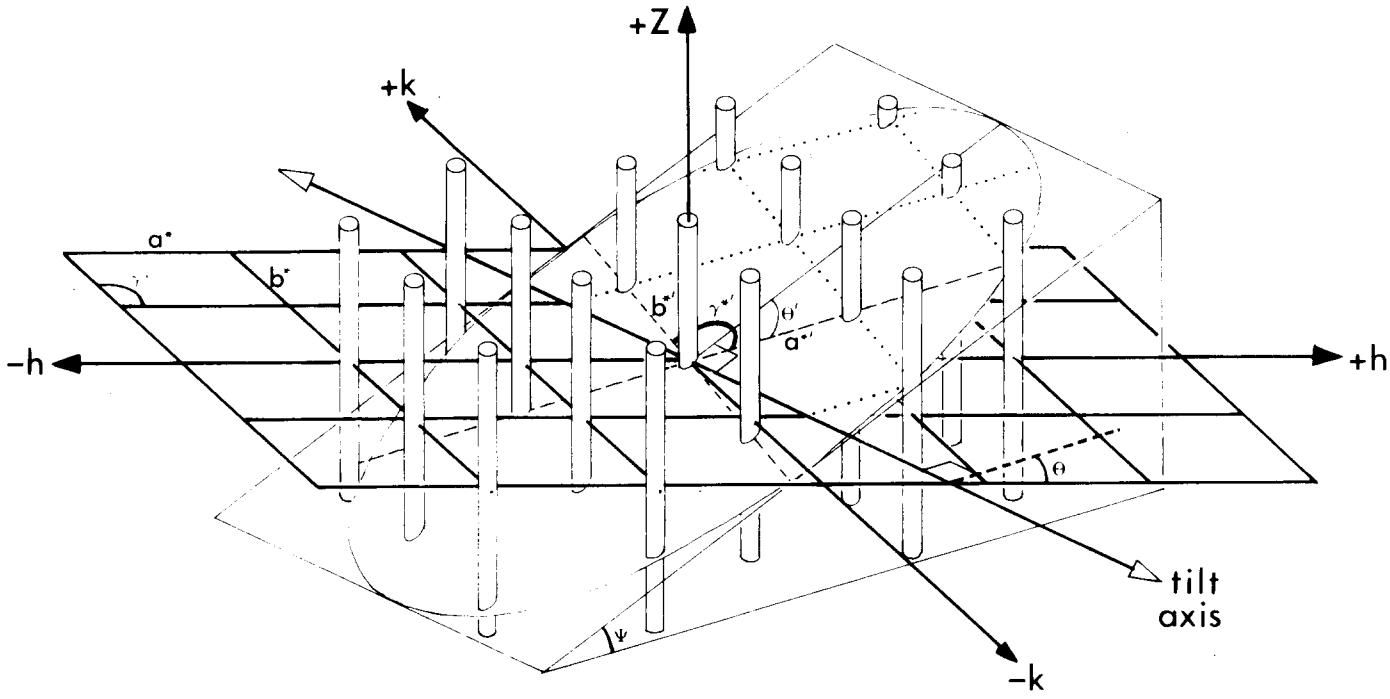

Figure 1 Intersection of a plane with the intensity distribution (represented as solid rods) in the three-dimensional diffraction pattern of a Zn-tubulin sheet, effectively a crystal one unit cell thick in one dimension. The intensities on the tilted plane represent the two-dimensional diffraction pattern of a particular projected view of the three-dimensional structure, in which the protofilaments lie at an angle θ' to the tilt axis, after being tilted through angle ψ from the normal. The indexing in two directions in reciprocal space (h, k) is as defined for the normal projection[10]. (It applies to a unit cell in the crystal with dimensions a = 9.8 nm, corresponding to the spacing of pairs of protofilaments, and b = 8 nm, the axial repeat of the tubulin dimers.) The third dimension in reciprocal space is defined by the continuous variable, Z. The labelling of the axes was chosen to follow other studies of tubulin protofilament structure[9-11,18] and does not correspond to that conventionally used in crystallography for $P2_1$ symmetry. With our conventions the symmetry of the structure requires the following phase (φ) and amplitude (|F|) relations:

$$\left.\begin{aligned}\varphi(h, k, Z) &= h\pi - \varphi(-h, k, Z)\\ |F|(h, k, Z) &= |F|(-h, k, Z)\end{aligned}\right\} \quad (1)$$

Thus, for $h = 0$, $\varphi = 0$ or π. Furthermore, for $k = 0$:

$$\left.\begin{aligned}\varphi(h, 0, Z) &= h\pi + \varphi(h, 0, -Z)\\ |F|(h, 0, Z) &= |F|(h, 0, -Z)\end{aligned}\right\} \quad (2)$$

have sought to sample the lines, out to points corresponding to nm resolution, at intervals of no more than 1/30 nm^{-1}. The data, which include 10 images at 21° tilt, 19 at 35° and 11 at 51°, actually contain sufficient redundancy that most of the interpolated values at 1/30 nm^{-1} intervals are derived from several different independent values (see Results, and *Figures* 4*a–i*); thus, a significant fraction of any noise should have been averaged out.

The redundancy in the data also assisted in finding the common phase origin in each image, by a comparison of the phase of each lattice point with those of neighbouring sample points from other images. Some of the images needed to be turned upside-down to agree with the others, in which case the tilt angle ψ in equations 3–5 became $-\psi$. The less tilted views were first correlated with the original untilted data (phases shown in *Table* 1) and views at higher tilt angles were subsequently incorporated into the collection (cf. Reference 13).

After all the tilt data had been gradually collected in this way, a few cycles of refinement of the phase origin in each image were carried out to produce the smoothest combination of data along all the various (h, k, Z) lines (using a weighted least-squares fit). At the same time, an amplitude scaling factor for the transform of each image was calculated, to give the best agreement with average neighbouring values of amplitude. A single scaling factor for all the lattice points in the transform of an individual image was used, since there were insufficient reflections per image to allow relative scaling of the transform in radial shells. Finally, after scaling of the amplitude values, smoothly-varying interpolated complex values were calculated at regular intervals (1/30 nm^{-1}) along each transform line from a simple distance-weighted average of all samples in the vicinity, i.e., using the symbols defined in *Figure* 1:

$$F(h, k, Z)\exp(i\varphi) = 1/N\sum_j F_j \exp(i\varphi_j)\sin(\pi d(Z-Z_j))/(\pi d(Z-Z_j))$$

summed between $(Z-0.033)$ and $(Z+0.033)$; N is the number of samples in this region. The nominal thickness of the sheet in the z-direction is d = 10 nm. In calculating the interpolated values, samples from the original Z = 0

Table 1 Summary of data in reciprocal space

		at $Z=0$*			
h	k	Relative amplitude	Relative phase ($\pm$RMS)	3-D data	RMS-3D
0	0			+	
1	0			+	42
2	0	850	0 ($\pm$1)	+	12
3	0			+	12
4	0	250	236 ($\pm$4)	+	22
6	0	106	30 ($\pm$10)		
0	1	78	0 ($\pm$16)		
3	1	66	50 ($\pm$24)		
0	2	158	0 ($\pm$9)	+	14
1	2	302	338 ($\pm$5)	+	21
2	2	135	290 ($\pm$8)	+	19
3	2	135	324 ($\pm$12)	+	25
4	2	91	53 ($\pm$22)		
5	2	72	196 ($\pm$29)		
6	2	63	245 ($\pm$37)		
0	3	96	0 ($\pm$7)		
1	3	71	314 ($\pm$23)		
2	3	85	136 ($\pm$20)		
3	3	69	227 ($\pm$16)		
1	4	110	185 ($\pm$10)		
2	4	78	77 ($\pm$20)		
3	4	104	64 ($\pm$21)		

* Data on the $Z=0$ plane were derived by enforcing perfect $P2_1$ symmetry on the values published by Baker & Amos[10]; RMS values are the root mean square errors in the relative phases. The indexing of h and k is as defined previously[10] – see *Figure* 1. +, in the column headed 3-D data indicates that a plot showing how this reflection varies with Z is included in *Figure* 4 (except for $h=0$, $k=0$, which can be seen in *Figure* 5*e*; other terms, which were already relatively weak, were found to fall rapidly to noise level away from $Z=0$. RMS-3D was calculated for each lattice line (see *Figure* 4) from $\{\Sigma|F|^2\Delta\Phi^2/\Sigma|F|^2\}$ where $\Delta\Phi$ represents the difference between an individual sample phase and the corresponding smoothed interpolated value and $|F|$ is the interpolated amplitude at that point. The overall weighted RMS phase difference for *all* the tabulated data is 17 ; this can be compared with a weighted RMS value of 8 for just the $Z=0$ data

data, being derived from an average of four highly selected images, were given eight times the weight of samples from individual tilted images. Furthermore, a final smoothing was applied by eye to some parts of the curves, where the large amplitude scatter mentioned in the Results section still gave rise to too rapid fluctuations in the interpolated values. Attempts to perform the interpolation by fitting a series of $\sin(\pi dZ)/(\pi dZ)$ functions to the values along each line had earlier been abandoned because of the large amplitude variations at different sample points.

Incorporation of data from images of sectioned sheets

Selected images of sectioned sheets which showed recognisable views (see Results) were also digitised and their Fourier transforms calculated; these provided continuous transform values along certain of the (h, k, Z) lines. In some cases, such samples overlapped data already obtained from tilted images, so that a relative amplitude scaling factor could be estimated for the two types of data. Scaled values for lines (0, 0, Z) and (1, 0, Z) which were not sampled by tilting, were extracted from the transforms of a number of images of sections and added to the 3-D data set (see *Figure* 4*a* and *b*).

Three-dimensional image reconstruction

Three-dimensional Fourier maps were calculated using a program written by G. Reeke, the maps being produced in the form of contoured sections, drawn by a Calcomp plotter[10]. A three-dimensional balsa-wood model was constructed from one of the contour levels.

Results

Images and optical diffraction patterns

As described under Experimental, it was found to be fairly easy to determine the relative orientations of

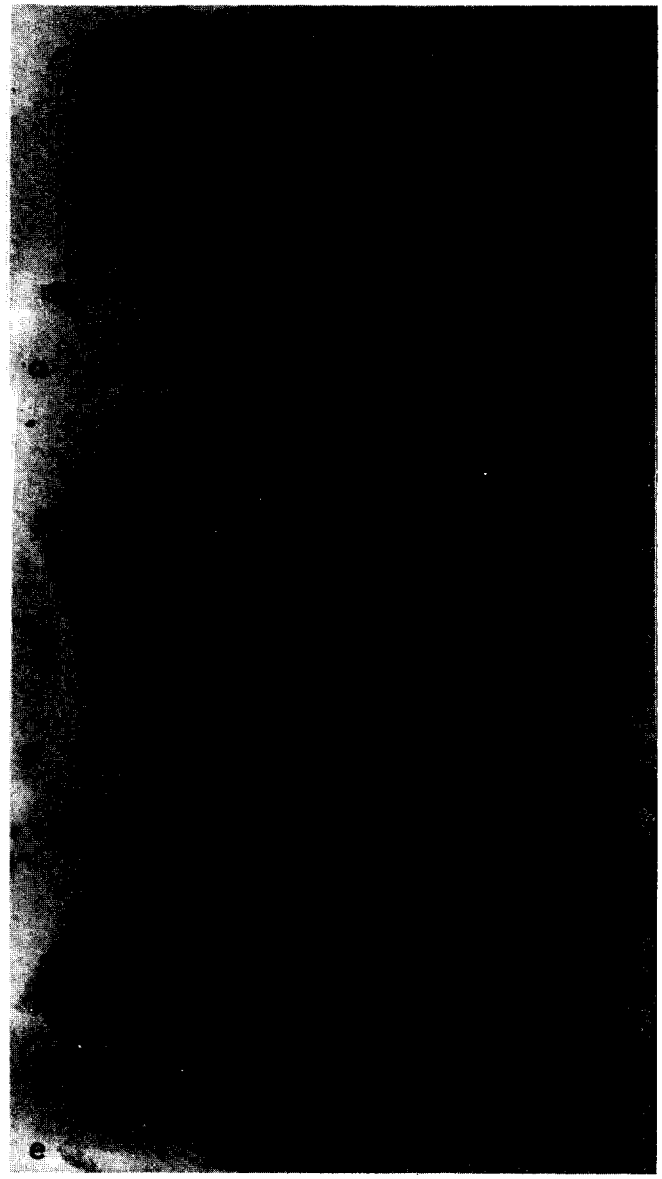

Figure 2 Electron micrographs of zinc-induced tubulin sheets, negatively stained with 1% uranyl acetate and recorded with minimal electron doses (see Reference 10). In these positive images, stain appears dark, while protein, revealed by absence of stain, appears to be white. The specimens were tilted relative to the electron beam: (a) was tilted through 35 ; (c) and (e) through 51 . (b), (d) and (f) show parts of (a), (c) and (e), respectively, at higher magnification (× 200,000). The direction of the tilt axis is marked by broken lines in each image, together with the angle θ' between the tilt axis and the projected protofilament axes in (a), (c) and (e). The protofilaments are aligned vertically in (b), (d) and (f). The outlined areas in (a), (c) and (e) are 200 nm squares which were densitometered as 512 × 512 point arrays for digital processing

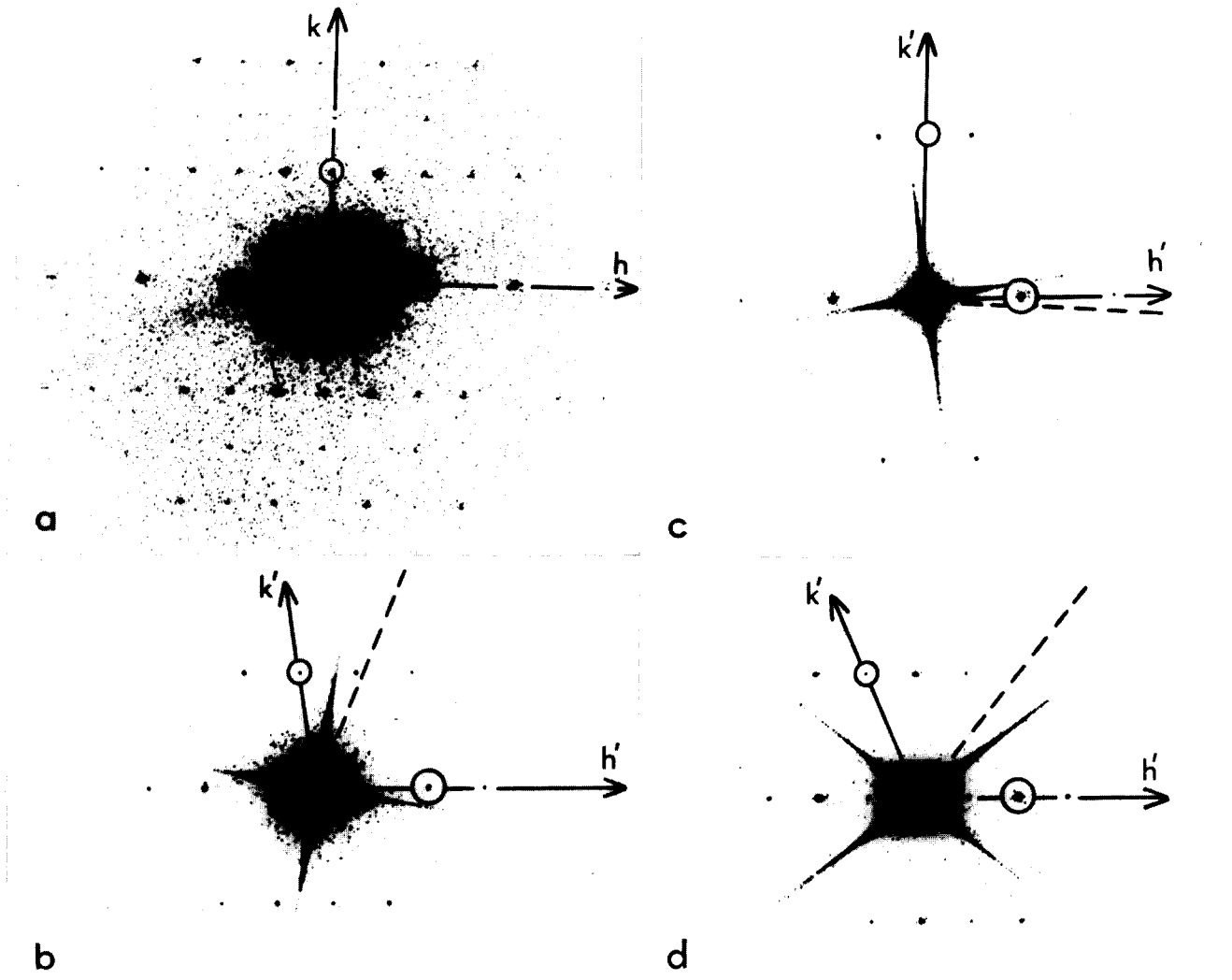

Figure 3 Optical diffraction patterns from rectangular regions of zinc-tubulin sheets, including those shown in *Figure* 2; protofilament axes were oriented vertically in each case. The axes labelled h and k are as shown in *Figure* 1. Reflections ($h = 2\ k = 0$) and ($h = 0, k = 2$) are ringed in each pattern. (a) is from an untilted sheet (*cf.* Reference 10); (b) was tilted through 35° (*cf. Figure* 2*a*); (c) and (d) were tilted through 51° (cf. *Figures* 2*c* and *e*). The broken lines in (b)–(d) show the direction of the tilt axis in each case

individual specimens randomly oriented on tilted electron microscope grids, even in highly tilted views (see *Figure* 2). Thus, the lattice points in the optical diffraction patterns (e.g. *Figures* 3*b–d*) were readily indexed, without requiring a tilt series of views for each specimen.

Because of the $P2_1$ symmetry[10] of the structure, lines of maxima in the three-dimensional Fourier transform at (h, k, Z) and ($-h$, k, Z) are closely related (see *Figure* 1), and data from them may be combined. It was found that, of the maxima appearing on the Z = 0 plane (see *Figure* 3*a*), only the six strongest related pairs (and their Friedel-related maxima) remained above noise level for a significant distance from that plane (see *Table* 1). The intensity of the other (weaker) maxima dropped quite rapidly to noise level and could not be measured in most of the tilted transforms. This was true for all reflections with odd values of k, arising from the small differences between the two types of tubulin monomer subunits, which alternate along the protofilaments[10]. However, two additional reflections (1, 0, Z) and (3, 0, Z), absent on the Z = 0 plane in accordance with the $P2_1$ symmetry, appear quite distinctly in the tilted transforms (see *Figures* 3*c* and *d*).

Data curves for (h, k, Z) lines

Of the eight independent reflections which are above noise level away from the Z = 0 plane, all but (1, 0, Z) and (1, 2, Z) faded out within the tilt range covered. (1, 0, Z) had in fact only just begun to appear and was relatively weak, while the intensity of (1, 2, Z) had fallen to about 0.25 of its maximum value. This meant that only data for (1, 0, Z) and (0, 0, Z) (which had been sampled only at Z = 0) were seriously missing from the 2 nm data obtained from tilted views.

When the relative phase origins had been refined and the polar orientations of the images had been chosen to give the best agreement between data from different micrographs (see Experimental), the sampled phases along each lattice line gave the curves shown in *Figure* 4. There is a fair amount of scatter in the individual values, especially at points where the amplitudes are relatively low, but the average values for each lattice line follow a smoothly varying curve. The weighted root mean square differences between the phases of the interpolated values and the individual sample values are listed in *Table* 1 for each of the strong lattice lines. As expected, the average phase errors are lower for the stronger lattice lines.

Even after the application of an overall amplitude scaling factor for each image, however, the amplitudes along the (h, k, Z) lines tend to show rather a large amount of scatter, much more than for the phases (see *Figure* 4).

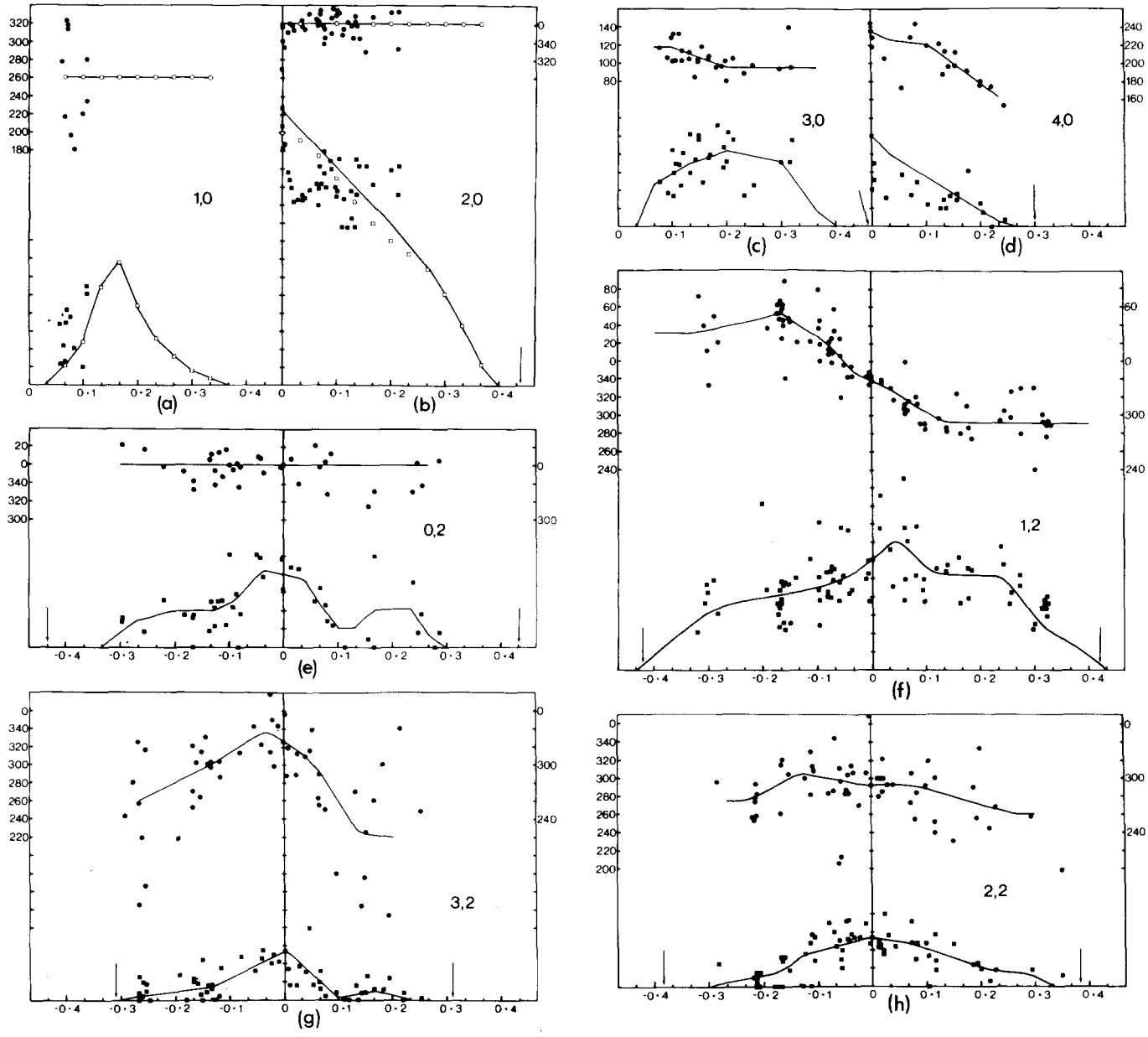

Figure 4 The relative phases in degrees (upper plot in each section) and amplitude values on an arbitrary, but consistent, scale (lower plots) along the main lattice lines of the three-dimensional Fourier transform of a Zn-tubulin sheet. Indices h and k (cf. *Figure* 1) are indicated in each plot. Values along the abscissae are reciprocal nm and represent the distance Z along the axis normal to the h and k axes. Note that values at $\pm Z$ are related for lines with $k = 0$ (plots (a)–(d)), as described under Experimental. Arrows indicate the cut-off point along each line corresponding to 2 nm resolution. Sample values derived from the computed Fourier transforms of individual images of tilted sheets are shown as filled circles (phases) and filled squares (amplitudes). The phase values are those obtained after refinement of the phase origin in each image to give the best overall agreement with the average. The amplitudes plotted are those obtained after relative scaling of whole individual transforms (see Experimental). Empty circles (phases) and empty squares (amplitudes) in (a) and (b) show values obtained by analysing images of sections normal to the sheets. The phase origins were chosen and the amplitudes scaled to match the tilt data by comparing common data on (1, 0, Z), (2, 0, Z) and (1, 2, Z) (section data not shown in last case). Amplitudes for (0, 0, Z) were similarly scaled. The continuous lines represent the smoothed interpolated values along each lattice line, obtained by averaging the complex values at nearby sample points. The overall errors in the interpolated phases on each lattice line are indicated in *Table* 1

This seems to be a common feature of data from negatively stained images (see e.g. Reference 17). The extent of the scatter seems to be more or less independent of the absolute value of the amplitude. Fortunately, the reconstructed image is rather less sensitive to errors in amplitude than to phase errors.

Data from sections

As mentioned above, the data obtained by tilting lack values in reciprocal space in a conical zone around the Z-axis. Without these data, the resolution in the reconstructed image would be anisotropic and features in the map would be smeared in the direction normal to the sheets. Images of sections normal to the plane of the sheets were used to explore the missing volume of reciprocal space. To ensure that the two types of data would be as consistent as possible, specimens were negatively stained before being embedded in plastic, rather than being positively stained after sectioning. Most of the images obtained showed only the overall stain distribution from

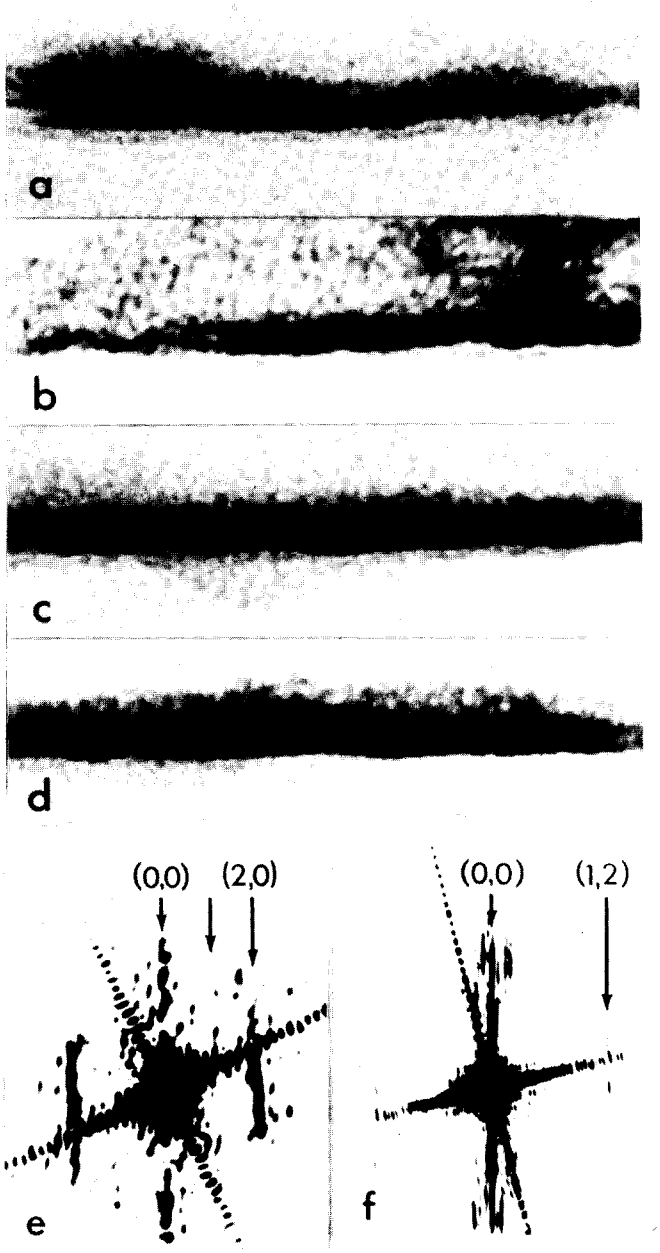

Figure 5 (a)–(d) Examples of images of sections cut normal to negatively stained Zn-tubulin sheets supported on carbon coated grids. The sheets show up as pairs of parallel lines of negative stain. The images are oriented so that the carbon film is below each specimen. In some cases, the sheets show some substructure, as in (a) and (b), which illustrate the two classes of identifyable image (see text); the spacing of the transverse striations in (b) is about 2/3 that in (a). (e) and (f) are optical diffraction patterns of (a) and (b) respectively. Notice the meridional (0, 0, Z) transform line in both cases. The strong non-meridional line of intensity in (e) is thought to be (2, 0, Z) (cf. *Figure* 4*b*), while the weaker line in (f) probably represents (1, 2, Z) (i.e. *Figure* 4*f*)

one side of a sheet to the other (providing data for the (0, 0, Z) line in reciprocal space), but a small number of more distinct views was obtained, as shown by the examples in *Figures* 5*a* and *b*. The two classes of distinctive view which were identified are thought to represent sections normal to the protofilaments (*Figure* 5*a*), providing data for the (*h*, 0, Z) lines, and normal to the transverse 4 nm oblique striations (*Figure* 5*b*) observed in normal views of Zn-tubulin sheets[7,10] providing data for the (1, 2, Z) transform line.

It was observed that the sections apparently shrink after they have been cut, as the measurements obtained from them are consistently 20% less than those obtained for the same dimensions in unsectioned sheets viewed face on. The shrinkage could not have occurred during embedding since the copper support grids were then still intact. Also, it seems unlikely that the discrepancy could be due to a misinterpretation of the distinctive views obtained. Possibly, the net shrinkage would have been less if the sections had been spread out on the water bath of the microtome, by the application of organic solvent vapour; the latter was not done as it caused most of the sections to split along the line of the grid. However, it should be pointed out that the measurements in question were in directions parallel, not normal, to the knife edge.

Optical transforms of images of sections (e.g. *Figure* 5*e*) suggest that the missing (1, 0, Z) line is of considerably weaker amplitude than the (2, 0, Z) line and could possibly be ignored. However, values for the amplitude and phase distributions on (1, 0, Z) were extracted from the computed Fourier transform of *Figure* 5*a* and were included in the data for completeness (see *Figure* 4*a*). The most important information from the sectioned views relates to the overall stain distribution (0, 0, Z), as this is completely unsampled in the tilted views. It is clear that the stain lies mainly in two layers on either side of the sheets, with a minimum stain density occurring in the central plane of the sheet: the strongest intersubunit connections, therefore, are probably found in the central plane. The total thickness of the stain–protein–stain sandwich appears to be only about 5 nm, although there is some indication of additional material extending beyond the upper layer of stain. Some of this probably represents non-tubulin associated proteins (see Discussion), but there may also be fine extensions from the tubulin subunits.

The reconstructed image

The overall resolution of the Fourier map calculated from the combined data (*Table* 1 and *Figure* 4) is about 2 nm; data on the Z=0 plane actually go out to 1.6 nm resolution[10], but away from this plane the intensity along most of the transform lines fades to noise level even before the 2 nm resolution limit is reached. This sort of limit to the resolution is what one would expect for negatively stained specimens.

The main features of the reconstructed density distribution and its relation to the projected image (*Figure* 6*a*) are shown in *Figures* 6*b–i* and 7. The two exposed surfaces of each protofilament are very different in appearance, one being smoothly rounded, the other much flatter and marked by a longitudinal groove down its centre. As a result, the protofilaments have a blunt spearhead shape in cross-section (*Figure* 6*b*). The longitudinal division of the protofilaments at intervals of 4 nm into monomer subunits can be clearly detected on both surfaces, as can the slight differences which distinguish the two species of monomer in a tubulin dimer. The differences are fairly subtle, less than one might expect even from the small differences observed in projection (*Figure* 6*a*), suggesting that the latter are due mainly to a slight difference in the orientation of the two kinds of subunit. The greatest difference between monomers in the three dimensional structure occurs on the flatter surface, where each subunit is divided into two domains. One kind of subunit seems to be more deeply divided than the other.

The main stain-excluding region in the centre of each

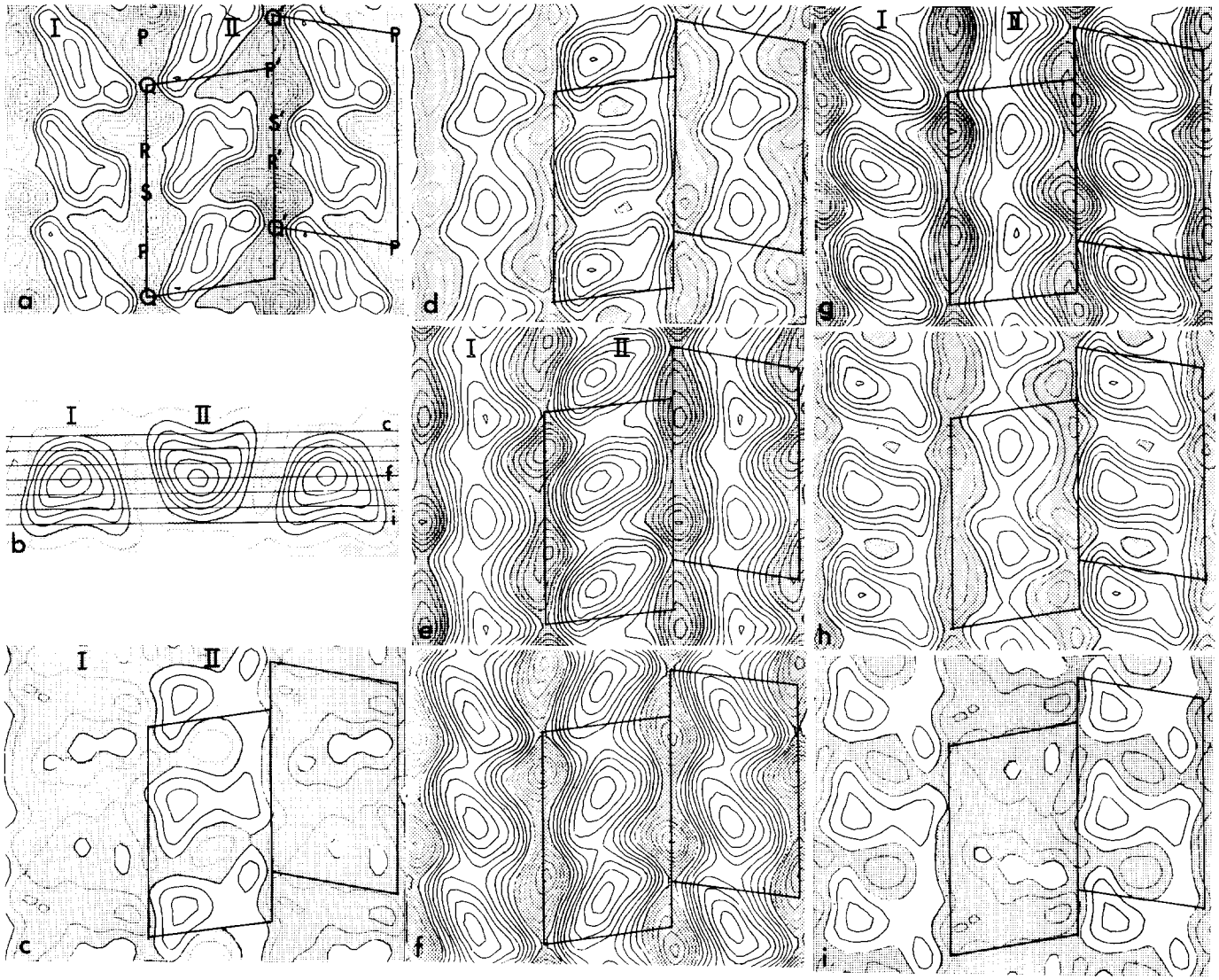

Figure 6 Projections, (a) and (b), and sections, (c) (i), through the reconstructed three-dimensional image of negatively stained Zn-tubulin sheets. (a) is a face-on projection of parts of 3 protofilaments. (b) is a projection down the protofilament axes: the positions of sections (c) (i) are indicated by horizontal lines in (b). The separation between adjacent planes (c) (i) is 0.6 nm. The variation in density is represented in each case by evenly spaced contour levels. Regions dominated by negative stain are shown shaded, while relative absence of stain (indicating the presence of protein) is represented by unshaded contours. Each globular unit at 4 nm intervals along a longitudinal protofilament is thought to represent a protein monomer of α or β-tubulin. The two boxes superimposed on every section each enclose what appears to be a single tubulin heterodimer. The axial repeat Q–Q is 8 nm and the boxes are 4.9 nm wide. Neighbouring protofilaments are related by $P2_1$ symmetry, about screw dyad axes normal to their own axes and in the central plane of the sheet. Features at the boundaries of the protofilaments are labelled in (a) to agree with the projected image shown by Baker & Amos[10].

subunit is roughly ellipsoidal and appears to be obliquely tilted relative to the protofilament axis in both face-on and side views. This can be seen by following the course of the contour peaks through the series of sections in *Figure* 6*c*–*i*. The obliquity of the subunits in projection (*Figure* 6*a*) has allowed a tentative identification[10] of the relative orientation of protofilaments in these sheets and in normal microtubules. The images labelled I in *Figures* 6 and 7 are thought to represent the view of a protofilament from the outside of a microtubule; in other words, the rounded side probably occurs on the outside surface of a microtubule and the flatter, grooved side on the inside surface. This identification is supported by the agreement between the appearances of the continuous ridged surface of the protofilaments in this structure and the outside of a three-dimensional reconstructed image of intact flagellar microtubules[1] (see later, *Figure* 8).

The interprotofilament contacts are clearly very much less extensive than the intraprotofilament bonds. On all the sections in *Figure* 6*c*–*i*, the stain density (shaded contour levels) thins out somewhere in the two regions P to Q and R to S. The region P to Q appeared in the two-dimensional projection (*Figure* 6*a*) to contain two distinct points of contact at P and Q[10] but a single broader area of contact seems more likely from the three-dimensional density distribution. Similarly a broad contact between R and S in the longitudinal direction is now suggested in place of a single contact point at the level of *R*.

Discussion

Good agreement between this three-dimensional image and images of negatively stained tubulin protofilaments in more normal structures confirms our earlier impression[10] that the substructure, and rotational orien-

tation about their axes, of protofilaments in zinc-induced sheets is very similar to that in microtubules. Comparison of the present model with images of normal tubulin assemblies has allowed us to identify the surfaces corresponding to the inside and outside of a normal microtubule[14]. As discussed in more detail elsewhere[14], the reconstructed image described here can readily be related to a number of different electron microscope images of tubulin protofilaments, which previously appeared to be rather disparate. The inner surface of the present protofilament model closely resembles the bilobed appearance of the two-dimensional images obtained by Erickson[18] (*cf. Figures* 8*a* and *b*), which were of opened out microtubules presumably stained most strongly on the inside surface. The projected image shown by Crepeau *et al.*[9], also of normal sheets, is probably similarly biased towards the appearance of the inside surface. On the other hand, as mentioned above, the three-dimensional image of flagellar microtubules reconstructed by Amos and Klug[1] bears a close resemblance to the outer surface of the present model protofilament structure. This is demonstrated in *Figures* 8*c* and *d* where the flagellar microtubule model is compared with a model constructed of Zn-tubulin protofilaments rearranged to conform to the normal polar structure of a microtubule. The flagellar model, being of rather low (4 nm) resolution, does not, however, show the same detail on its inner surface (not shown here) as the Zn-tubulin model and gives no indication of the longitudinal cleft down the centre of each protofilament. One reason for this may be that insufficient negative stain may reach the inside surfaces of intact microtubules.

The model shown in *Figure* 8*d* is also in good agreement with microtubule cross-sections observed in electron micrographs of embedded and sectioned material. A cross-sectioned view derived from the model (*Figure* 9*a*) agrees well with the clear electron microscope images resulting from pretreatment of the sectioned material with tannic acid[19,20] or thiourea[21], in which the interprotofilament connections appear to be at inner radii. The alternative arrangement of model protofilaments, with the wedge-shapes pointing inwards, has a quite different appearance in cross-section (*Figure* 9*b*), which does not agree with the electron microscope images.

The strong structural similarity between the three-dimensional images of the two kinds of monomer subunit is what one would expect from the apparently close homology between their sequences[22]. It is also consistent with the apparent ability of tubulin to assemble in two different dimer arrangements, with interprotofilament associations either between unlike monomer subunits, as in the case of the A-tubule of flagellar doublets[1] and flagellar central singlet tubules[23], or between like monomers, as in the case of the flagellar B-tubule[1].

The precise arrangement of tubulin dimers in a tubulin assembly may be determined by one or more of the so-called microtubule-associated proteins (MAPs) which co-purify with tubulin. These proteins were present in the preparations of zinc-induced tubulin sheets studied in the present work. But as pointed out previously[10], they may not make a significant contribution to the reconstructed image. This is because, although MAPs probably constitute about 25% of the total protein, only about 10% of each molecule is thought to be bound directly to tubulin[24], while the rest forms an apparently flexible filamentous projection[25,26] whose contribution should be averaged out of the data. The location of the bound portions of the MAPs (maybe only 2.5% of total protein) presents a difficult problem, which is probably insoluble using negatively stained specimens.

The structural results described here have been correlated in some detail[14] with the information available from X-ray diffraction: a calculated diffraction pattern for the rearranged model shown in *Figure* 8*d* being compared with the measured X-ray diffraction patterns obtained from oriented hydrated specimens[5,6]. The first obvious

Figure 7 (a) A model representing the three-dimensional reconstructed image of part of a Zn-tubulin sheet. Notice the different appearances of the surfaces presented by adjacent protofilaments. The boxes enclose pairs of monomer subunits as in *Figure* 6. In view I, the longitudinally continuous surface appears to be divided into monomer subunits consisting of single globular domains. In view II, monomer subunits separated by oblique channels each appear to be dissected sideways into two domains by longitudinal grooves. The relationship between the two surfaces can be seen more clearly in (b). (b) Two different side views of a length of protofilament equivalent the second from the left in (a). Individual monomer subunits probably slope up from left to right in the left-hand view and down in the right-hand view. This was deduced by following the regions of strongest density through successive sections in *Figure* 6

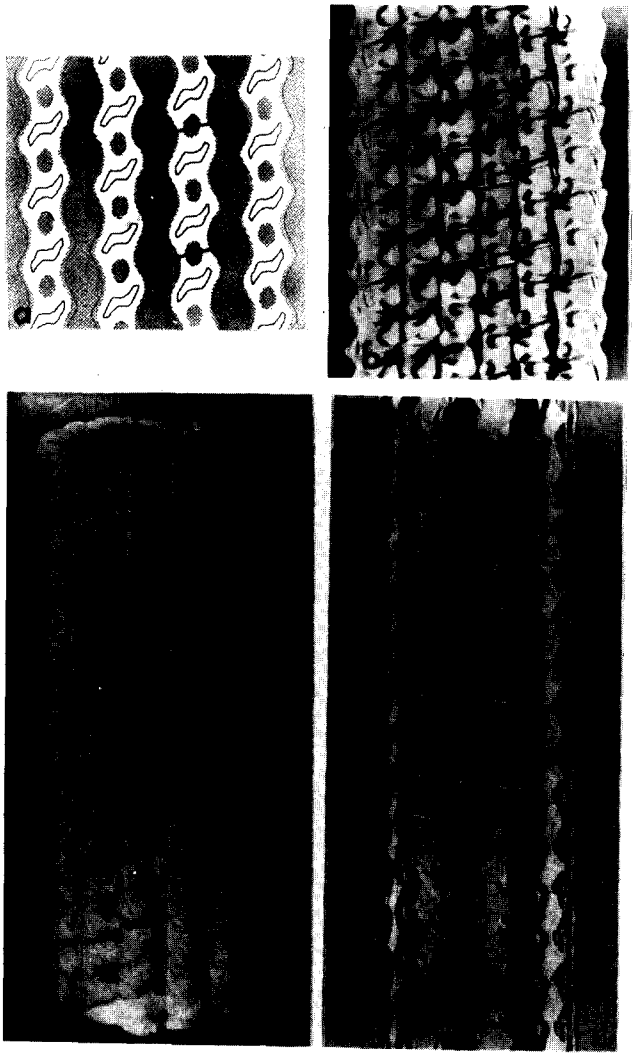

Figure 8 'Normal' arrangements of tubulin protofilaments; the boxes in each image enclose 8 nm long by 5 nm wide heterodimers as in *Figures* 6 and 7. (a) Two-dimensional image of part of a negatively stained opened-out brain microtubule, reconstructed from the data of Erickson[18]; the latter did not include any information about the weak 8 nm axial repeat which distinguishes the two kinds of monomer subunit. (b) Models of Zn-tubulin protofilaments (from *Figure* 7), rearranged to represent a C-shaped normal sheet. This corresponds to part of (d), opened-out and seen from the inside surface. (c) Model of an intact flagellar microtubule[1], in which the monomer subunits of the 13 protofilaments lie along a set of 3 shallow left-handed helices. Dimers (of which two are outlined) in adjacent protofilaments are in a staggered arrangement. The basal end of the flagellum would be towards the top of the model in this view. (d) Zn-tubulin protofilament models rearranged with the subunit arrangement in (c). The polarity of the protofilaments was chosen to give the best agreement between the two structures

difference in the two types of data is in the apparent depth of the protofilaments. Whereas the X-ray diffraction patterns have been interpreted in terms of a cylinder with inner and outer radii of 7 8 nm and 15 nm respectively, indicating a thickness of 7–8 nm, the negatively stained sheets appear to be only about 5 nm thick. This difference may arise partly from shrinkage of the stained specimens due to dehydration. Another likely effect, which would reduce the apparent dimensions, is positive staining of the protein surface. In particular, it is likely that the protruding longitudinal ridge on the outside surface of each protofilament is significantly reduced in apparent extent by such a positive staining effect. Conversely, the sizes of the stain-filled grooves on the 'inside' surface of the protofilaments are probably exaggerated.

The differences between the calculated diffraction pattern based on the structure of the negatively stained Zn-tubulin protofilaments and the measured X-ray diffraction pattern can mostly be explained in terms of effects such as these[14]. However, the detailed comparison suggested that negative stain tends particularly to overemphasize the oblique grooves on the 'inside' surface of the protofilaments, and the reason for this is not yet clear.

The remaining uncertainties in the structure at this resolution, due to the distorting effects of negative stain, may be resolvable by studying the three-dimensional structure of unstained specimens of tubulin sheets. The use of such specimens would also allow a better chance of making quantitative measurements and might therefore even lead to location of the MAPs by a comparison of the structures of sheets assembled with and without non-tubulin components. The possibility of such a study to suitably high resolution will depend on the preparation of sufficiently large and well-ordered sheets. Meanwhile, the

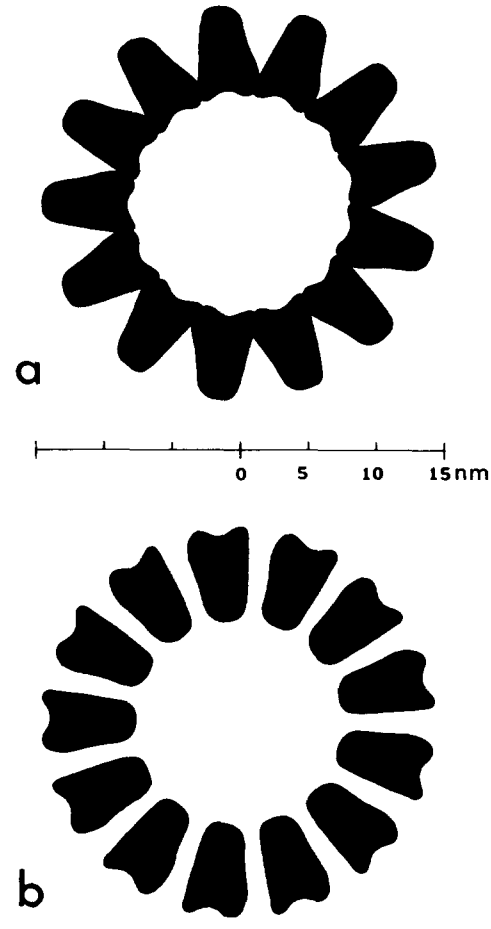

Figure 9 Projected views of short lengths of model protofilaments arranged to form a cylinder. The dimensions of the protofilaments were stretched radially by 40% to compensate for the apparent shrinkage in the z-direction of the original sheets (see text). (a) and (b) show two different possible orientations of the protofilaments, with either their rounded surfaces (a) or their flat surfaces (b) on the outside of the cylinder. As discussed in the text, (a) is believed to be the arrangement found in a normal microtubule (see also *Figure* 8*c* and *d*)

present three-dimensional map provides an image of tubulin which is more consistent with all available information than any previous individual image of tubulin.

Acknowledgements

The authors thank Drs R. Henderson, P. N. T. Unwin and A. Klug for helpful discussions and C. Villa for making models. This investigation has been aided by a grant from the Jane Coffin Childs Memorial Fund for Medical Research. During the course of the work, T.S.B. was a fellow of the Jane Coffin Childs Memorial Fund. We thank Dr. S. J. Edelstein for communicating to us, before publication, results of work in his laboratory: an independent image reconstruction of Zn-tubulin sheets[27] shows features very similar to ours.

References

1 Amos, L. A. and Klug, A. *J. Cell Sci.* 1974, **14**, 523
2 Amos, L. A., Linck, R. W. and Klug, A. *Cold Spring Harbor Confs. on Cell Proliferation* (Cell Motility) 1976 Vol. 3, 847.
3 Tsuprun, V. L., Stel'mashuk, V. Ya., Kiselev, N. A., Gelfand, V. I. and Rosenblat, V. A. *Mol. Biol. (USSR)* 1975, **10**, 360
4 Cohen, C., Harrison, S. C. and Stephens, R. E. *J. Mol. Biol.* 1971, **59**, 375
5 Cohen, C., DeRosier, D. J., Harrison; S. C., Stephens, R. E. and Thomas, J. *Ann. N. Y. Acad. Sci.* 1975, **253**, 53
6 Mandelkow, E., Thomas, J. and Cohen, C. *Proc. Natl. Acad. Sci. USA* 1977, **74**, 3370
7 Larsson, H., Wallin, M. and Edstrom, A. *Exp. Cell. Res.* 1976, **100**, 104
8 Gaskin, F. and Kress, Y. J. Biol. Chem. 1977, **252**, 6918
9 Crepeau, R. H., McEwen, B., Dykes, G. and Edelstein, S. J. *J. Mol. Biol.* 1977, **116**, 301
10 Baker, T. S. and Amos, L. A. *J. Mol. Biol.* 1978, **123**, 89
11 Crepeau, R. H., McEwen, B. and Edelstein, S. J. *Proc. Natl. Acad. Sci. USA* 1978, **75**, 5006
12 DeRosier, D. J. and Klug, A. *Nature* 1968, **217**, 130
13 Henderson, R. and Unwin, P. N. T. *Nature* 1975, **257**, 28
14 Amos, L. A. and Baker, T. S. *Nature* 1979, **279**, 607
15 Unwin, P. N. T. and Henderson, R. *J. Mol. Biol.* 1975, **94**, 425
16 Erickson, H. P. and Klug, A. *Philos. Trans. R. Soc. London, Ser B.* 1971, **261**, 105
17 Henderson, R., Capaldi, R. and Leigh, J. S. *J. Mol. Biol.* 1977, **112**, 631
18 Erickson, H. P. *J. Cell Biol.* 1974, **60**, 153
19 Tilney, L. G., Bryan, J., Bush, D. J., Fujiwara, K., Mooseker, M., Murphy, D. and Snyder, D. M. *J. Cell Biol.* 1973, **59**, 267
20 Pierson, G. B., Burton, P. R. and Himes, R. H. *J. Cell Biol.* 1978, **76**, 223
21 Warner, F. D. and Satir, P. *J. Cell Sci.* 1974, **12**, 313
22 Luduena, R. F. and Woodward, D. O. *Proc. Natl. Acad. Sci. USA* 1973, **70**, 3594
23 Chasey, D. *Exp. Cell Res.* 1972, **74**, 140
24 Vallee, R. B. and Borisy, G. G. *J. Biol. Chem.* 1977, **252**, 377
25 Dentler, W. L., Granett, S. and Rosenbaum, J. L. *J. Cell Biol.* 1975, **65**, 237
26 Murphy, D. B. and Borisy, G. G. *Proc. Natl. Acad. Sci. USA* 1975, **72**, 2696
27 Tamm, L. K., Crepeau, R. H. and Edelstein, S. J. *J. Mol. Biol.* 1979, **130**, 473